Deposition of Antimony Sulfide Thin Films from Single-Source Antimony Thiolate Precursors

Jorge Rodriguez-Castro, Phillip Dale, Mary F. Mahon,* Kieran C. Molloy,* and Laurie M. Peter

Department of Chemistry, University of Bath, Claverton Down, Bath, BA2 7AY, United Kingdom

Received February 9, 2007. Revised Manuscript Received April 24, 2007

Antimony sulfide thin films have been deposited for the first time by MOCVD using antimony thiolates $Sb(SR)_3$ (R = Bu^t (**1**), CH_2CF_3 (**2**)) as single-source precursors. The structure of **1** was determined by X-ray crystallography and shown to be a monomer. Films were grown from **1** and **2** by low-pressure CVD using both glass slides and silicon wafers as substrates, at substrate temperatures of 300 and 450 °C, respectively. In both cases, the deposited films exhibited XRD patterns that could be fully indexed to orthorhombic stibnite, with stoichiometries in the range $Sb_2S_{2.78-3.10}$ by EDXS. In addition, there is evidence for the formation of small amounts of antimony metal in the films derived from **2**. The morphologies of the films are strongly substrate dependent: **1** generates random platelets regardless of substrate, whereas **2** deposits a uniform film with islands of needle morphology on glass or long rods of stacked platelets on Si. A film deposited on glass is photoactive and has a band gap of 1.6 eV.

1. Introduction

There is considerable current interest in the synthesis of binary 15−16 materials in both nanocrystalline and thin film forms, as a result of their diverse materials' properties and hence applications. Recent reports include the growth of Bi_2S_3,[1−3] Bi_2Te_3,[4−7] Sb_2Se_3,[8,9] and Sb_2Te_3.[10,11] Our current interest among these binary materials is antimony sulfide (stibnite, Sb_2S_3), a potentially useful material with applications in such diverse areas as thermoelectric devices,[12] solar cells,[13] television cameras,[14] microwave,[15] and switching devices.[16] It is a weakly polar semiconducting ferroelectric that can undergo phase transitions accompanied by small structural changes in the coordination sphere of the antimony centers.[17] The band gap of Sb_2S_3 is between 1.78 and 2.5 eV, covering the maximum scan of the visible and near-infrared ranges of the solar spectrum.[18−20]

Preparative routes to Sb_2S_3 have included chemical bath deposition,[20−22] hydro- or solvothermal synthesis,[23−25] and refluxing[26] or microwave treatment[27] of various precursors[28] dissolved in polyols. Deposition of thin films of Sb_2S_3 are largely limited to reports on spray pyrolysis[29,30] and vacuum evaporation approaches,[31,32] although we have reported recently[33] on an aerosol-assisted CVD (AACVD) route using unsymmetrical antimony(III) dithiocarbamates. This latter study highlighted a key problem for any CVD approach to

* To whom correspondence should be addressed. E-mail: chskcm@bath.ac.uk (K.C.M.).

(1) Koh, Y. W.; Lai, C. S.; Du, A. Y.; Tiekink, E. R. T.; Loh, K. P. *Chem. Mater.* **2003**, *15*, 4544.
(2) Monteiro, O. C.; Trindade, T.; Park, J. H.; O'Brien, P. *Chem. Vap. Deposition* **2000**, *6*, 230.
(3) Monteiro, O. C.; Trindade, T.; Park, J. H.; O'Brien, P. *Mater. Lett.* **2004**, *58*, 119.
(4) Kim, D. H.; Byon, E.; Lee, G. H.; Cho, S. *Thin Solid Films* **2006**, *510*, 148.
(5) Purkayastha, A.; Lupo, F.; Kim, S.; Borca-Tasciuc, T.; Ramanath, G. *Adv. Mater.* **2006**, *18*, 496.
(6) Zhou, B.; Zhao, Y.; Pu, L.; Zhu, J. J. *Mater. Chem. Phys.* **2006**, *96*, 192.
(7) Li, S.; Toprak, M. S.; Soliman, H. M. A.; Zhou, J.; Muhammed, M.; Platzek, D.; Muller, E. *Chem. Mater.* **2006**, *18*, 3627.
(8) Yu, Y.; Wang, R. H.; Chen, Q.; Peng, L. M. *J. Phys. Chem. B* **2006**, *110*, 13415.
(9) Rodriguez-Lazcano, Y.; Pena, Y.; Nair, M. T. S.; Nair, P. K. *Thin Solid Films* **2005**, *493*, 77.
(10) Garje, S. S.; Eisler, D. J.; Ritch, J. S.; Afzaal, M.; O'Brien, P.; Chivers, T. *J. Am. Chem. Soc.* **2006**, *128*, 3120.
(11) Wang, W. Z.; Poudel, B.; Yang, J.; Wang, D. Z.; Ren, Z. F. *J. Am. Chem. Soc.* **2005**, *127*, 13792.
(12) Kim, I. H. *Mater. Lett.* **2000**, *43*, 221.
(13) Rajpure, K. Y.; Bhosale, C. H. *Mater. Chem. Phys.* **2000**, *64*, 70.
(14) Cope, D. U.S. Patent 1959, 2875359.
(15) Grigas, J.; Meshkauskas, J.; Orliukas, A. *Phys. Status Solidi A* **1976**, *37*, K39.
(16) Ablova, M. S.; Andreev, A. A.; Dedegkaev, T. T.; Melekh, B. T.; Pevtsov, A. B.; Shendel, N. S.; Shumilova, L. N. *Sov. Phys. Semicond.−USSR* **1976**, *10*, 629.
(17) Rinkyavichyhs, V. S.; Mikalkevichyus, M. P. *Phys. Status Solidi A* **1968**, *9*, 2360.
(18) Deshmukh, L. P.; Holikatti, S. G.; Rane, B. P.; More, B. M.; Hankare, P. P. *J. Electrochem. Soc.* **1994**, *41*, 1779.
(19) Savadogo, O.; Mandal, K. C. *Sol. Energy Mater.* **1992**, *26*, 117.
(20) Nair, M. T. S.; Pena, Y.; Campos, J.; Garcia, V. M.; Nair, P. K. *J. Electrochem. Soc.* **1998**, *145*, 2113.
(21) Mane, R. S.; Lokhande, C. D. *Mater. Chem. Phys.* **2003**, *82*, 347.
(22) Salem, A. M.; Selim, M. S. *J. Phys. D: Appl. Phys.* **2001**, *34*, 12.
(23) Wang, J. W.; Li, Y. D. *Mater. Chem. Phys.* **2004**, *87*, 420.
(24) Hu, H.; Liu, Z.; Yang, B.; Mo, M.; Li, Q.; Yu, W.; Qian, Y. *J. Cryst. Growth* **2004**, *262*, 375.
(25) Hu, H.; Mo, M.; Yang, B.; Zhang, X.; Li, Q.; Yu, W.; Qian, Y. *J. Cryst. Growth* **2003**, *258*, 106.
(26) Zhang, R.; Chen, X.; Mo, M.; Wang, Z.; Zhang, M.; Liu, X.; Qian, Y. *J. Cryst. Growth* **2004**, *262*, 449.
(27) Chen, D.; Tang, K.; Shen, G.; Sheng, J.; Fang, Z.; Liu, X.; Zheng, H.; Qian, Y. *Mater. Chem. Phys.* **2003**, *82*, 206.
(28) An, C. H.; Tang, K. B.; Yang, Q.; Qian, Y. T. *Inorg. Chem.* **2003**, *42*, 8081.
(29) Rajpure, K. Y.; Bhosale, C. H. *J. Phys. Chem. Solids* **2000**, *61*, 561.
(30) Rajpure, K. Y.; Bhosale, C. H. *Mater. Chem. Phys.* **2002**, *73*, 6.
(31) El Zawawi, I. K.; Abdel-moez, A.; Terra, F. S.; Mounir, M. *Thin Solid Films* **1998**, *324*, 300.
(32) El-Shazly, A. A.; Belal, A. E.; Nigim, A. A.; Abdul Masih, G. *Opt. Pura Apl.* **1981**, *14*, 129.
(33) Rodriguez-Castro, J.; Mahon, M. F.; Molloy, K. C. *Chem. Vapor Deposition* **2006**, *12*, 601.

10.1021/cm070405j CCC: $37.00
Published on Web 06/05/2007

Sb_2S_3: films grown at temperatures in excess of ca. 300 °C show a strong tendency to incorporate oxygen; in the case of AACVD, it is either from traces of oxygen in the N_2 carrier gas or from the solvent. Our solutions to this problem are 2-fold: identify either precursors that, unlike antimony dithiocarbamates, decompose readily at $T < 300$ °C or, again unlike the dithiocarbamates, precursors of sufficient volatility to be used in low-pressure CVD (LPCVD) where the available oxygen is minimized. We will report elsewhere on the use of antimony xanthates as precursors for low-temperature AACVD,[34] whereas in this report, we detail the use of volatile antimony thiolates for the deposition of Sb_2S_3 by LPCVD.

2. Experimental Section

Elemental analyses were performed using an Exeter Analytical CE 440 analyzer. ^{1}H and ^{13}C NMR spectra were recorded on a Bruker Advance 300 MHz FT−NMR spectrometer as saturated solutions at room temperature; chemical shifts are in parts per million with respect to either Me_4Si; coupling constants are in hertz. SEM was carried out on a JEOL JSM-6310 microscope, whereas quantitative EDXS measurements were made on a JEOL JXA-8600 electron probe microanalyzer. XRD was performed using a Bruker D8 diffractometer on which coupled $\theta-2\theta$ scans were carried out. Thermogravimetric studies were performed on a Perkin-Elmer TGA7 analyzer; samples were loaded as quickly as possible in air and the temperature was then increased under a flow of dry N_2 gas.

Synthesis. Starting materials were commercially obtained (e.g., Aldrich) and used without further purification unless otherwise stated. Standard Schlenck line techniques were employed where applicable.

*Synthesis of Antimony(III) Tris(t-butylthiolate), Sb(SBu^t)$_3$ (**1**):* A solution of sodium *tert*-butylthiolate (0.74 g, 6.6 mmol) in methanol (30 mL) was added to a solution of $SbCl_3$ (0.5 g, 2.2. mmol) in methanol (20 mL), which resulted in the immediate formation of a white suspension. The mixture was allowed to stir overnight, after which time all volatiles were removed under a vacuum. The crude reaction product was redissolved in diethyl ether (60 mL) and filtered through Celite, resulting in a pale yellow solution. The solvent was evaporated and the remaining solid was washed with hexane (2 × 25 mL) and dried under vacuum, giving 0.60 g (70%) of **1** as a white solid. Mp: 150 °C (sublimes). Anal. Found (calcd) for $C_{12}H_{27}S_3Sb$: C, 37.90 (37.02); H, 6.45 (6.99). ^{1}H NMR (C_6D_6): δ 1.40 (27H, s, CH_3), ^{13}C NMR (C_6D_6): 47.0 [$C(CH_3)_3$], 35.9 [C(CH_3)$_3$].

*Synthesis of Antimony(III) Tris(2,2,2-trifluoroethanethiolate, Sb(SCH$_2$CF$_3$)$_3$ (**2**):* 2,2,2-Trifluoroethanethiol (1.17 mL, 13.2 mmol) was added dropwise to a solution of $SbCl_3$ (1.00 g, 4.4 mmol) in toluene (60 mL), resulting in a colorless solution. Ammonia was slowly bubbled through the reaction mixture, causing a white precipitate of NH_4Cl. This bubbling was continued until no more precipitate was formed. The NH_4Cl was separated by cannula filtration, and toluene evaporated from the filtrate under a vacuum to leave **2** (1.44 g, 70%) as a clear oil. Anal. Found (calcd) for $C_6H_6F_9S_3Sb$: C, 16.00 (15.42); H, 1.37 (1.29). ^{1}H NMR ($CDCl_3$): δ 3.40 (6H, q, CH_2), ^{13}C NMR ($CDCl_3$): 126.0 (q, $^1J_{C-F} = 276$ Hz, CF_3CH_2), 32.3 (q, $^2J_{C-F} = 33.9$ Hz, CF_3CH_2), ^{19}F-NMR ($CDCl_3$): −66.8 (t, $^3J_{H-F} = 9.8$ Hz, CF_3).

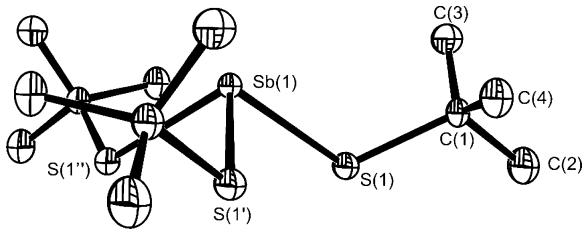

Figure 1. Structure of **1** showing the atom labeling scheme; ellipsoids are at the 30% probability level. Only the major component of the disordered structure is shown, and hydrogen atoms have been omitted for clarity. Sb(1)−S(1) 2.4248(14), S(1)−C(1) 1.852(6), C(1)−C(2) 1.510(8), C(1)−C(3) 1.489(9), C(1)−C(4) 1.541(7); S(1)−Sb(1)−S(1′) 91.63(6), C(1)−S(1)−Sb(1) 105.4(2), C(3)−C(1)−C(2) 110.9(6), C(3)−C(1)−C(4) 111.2(6), C(2)−C(1)−C(4) 109.6(5), C(2)−C(1)−S(1) 104.8(4), C(3)−C(1)−S(1) 109.5(4), C(4)−C(1)−S(1) 110.5(4). Symmetry transformations used to generate equivalent atoms: ′ $-y, x-y, z$; ″ $-x+y, -x, z$.

Table 1. Crystallographic Data Collection Parameters for 1

empirical formula	$C_{12}H_{27}S_3Sb$
fw	389.27
cryst syst	hexagonal
space group	$P6_3$
a (Å)	10.3430(2)
b (Å)	10.3430(2)
c (Å)	9.7560(3)
V (Å^3)	903.85(4)
Z	2
density (calcd) (mg/m^3)	1.430
abs coeff (mm^{-1})	1.852
max., min. transmission	0.866, 0.686
no. of reflns collected	19393
no. of independent reflns	1761 (R(int) = 0.0772)
no. of reflns observed (>2σ)	1273
final R_1, wR_2 [$I > 2\sigma(I)$]	0.0339, 0.0702
R_1, wR_2 indices (all data)	0.0637, 0.0792
Flack param	0.22(6)
largest diff. peak, hole (e Å^{-3})	0.644 and −0.598

X-ray Crystallography. Crystals of **1** were grown by sublimation; a crystal of dimensions 0.08 × 0.08 × 0.22 mm^3 was used for data collection. Crystallographic data for **1** are given in Table 1. Data were collected at 150(2) K on a Nonius Kappa CCD diffractometer using Mo-K$_\alpha$ radiation ($\lambda = 0.71073$ Å) to a $2\theta_{max}$ of 60.04° using the ω rotation scan mode and were corrected for Lorentz, polarization and absorption. The asymmetric unit of **1** contains 1/3 of a molecule with the central Sb atom located on a 3-fold rotation axis. The structure is disordered over 2 sites in a 3:1 ratio, which was initially misleading in terms of space group determination, as $P6_3/m$ had a reasonable level of credibility. All atoms were allowed to vibrate anisotropically, and hydrogen atoms were included at calculated positions. Structure determination and refinement (full matrix least-squares on F^2) was carried out using SHELX-86[35] and SHELX-93,[36] respectively; the asymmetric unit, shown in Figure 1 along with the labeling schemes used, relates only to the major component of the disorder and was produced using ORTEX.[37]

Low-Pressure Chemical Vapor Deposition Studies. Films were grown on a purpose-built hot-wall low-pressure CVD reactor, details of which are given elsewhere.[38] Pyrex slides were used as substrates and cleaned prior to use by washing successively with water/detergent and acetone. Silicon wafers, which were also used as substrates, were wiped clean with a dry cotton pad.

(34) Rodriguez-Castro, J.; Mahon, M. F.; Molloy, K. C.; Tiekink, E. R. T.; White, T. Unpublished results.

(35) Sheldrick, G. M. *SHELX-86*; University of Göttingen: Göttingen, Germany, 1986.

(36) Sheldrick, G. M. *SHELX-97*; University of Göttingen: Göttingen, Germany, 1993.

(37) McArdle, P. *J. Appl. Crystallogr.* **1994**, *27*, 438.

(38) Horley, G. A.; Mahon, M. F.; Molloy, K. C.; Haycock, P. W.; Myers, C. P. *Inorg. Chem.* **2002**, *41*, 5052.

Table 2. Conditions for the CVD of Sb_2S_3 Using Antimony (III) Thiolates

precursor	furnace *T* (°C)	substrate *T* (°C)	run time (h)	substrate slides	film color
1	130	300	2	glass	black
1	130	300	1	silicon	dark grey
2	150	450	0.5	glass	light grey
2	150	450	0.5	silicon	light grey

For each growth experiment, approximately 0.3 g of complex was used. For these experiments, the precursor was held at low pressure inside the quartz tube (ca. 0.1 mmHg) and heated in a tube furnace until volatilization was complete (usually leaving a residue of amorphous Sb_2S_3). At the same time, external to the furnace, the deposition substrate was independently heated by a ceramic infrared heater to the desired decomposition temperature. Additional experimental details are summarized in Table 2. ***Caution:*** *H_2S is a likely decomposition product of these experiments.*

All films adhered well to the substrates and could not be easily removed without scratching.

Opto-electronic Measurements. The opto-electronic properties of the films were investigated by photovoltammetry and photocurrent spectroscopy. Measurements were made using an electrolyte contact of 0.1 M Na_2SO_3 (aq) in a three-electrode cell equipped with a Ag|AgCl reference electrode and a platinum foil secondary electrode. The Sb_2S_3 film was deposited on TEC-10 glass, where the coated layer is fluorine-doped tin oxide. The active area of the electrode was masked with polyimide tape. The potential of the electrode was controlled by an Autolab PGSTAT12 computer-controlled potentiostat. For the photovoltammetry experiments, the electrode was illuminated by a high-power white LED, which was switched on for 1 s and off for 0.4 s while the potential of the electrode was scanned at 30 mV s^{-1} from −0.9 to +0.4 V vs Ag|AgCl. Photocurrent spectra were measured using chopped monochromatic light (chopping frequency 4 Hz) provided by a xenon lamp and monochromator. The potential of the electrode was held at +0.2 V vs Ag|AgCl and the photocurrent was detected using a digital lock-in amplifier (Stanford 830 DSP). The spectra were corrected for the incident photon flux, which was measured using a calibrated silicon diode traceable to NBS standard.

3. Results and Discussion

Synthesis and Characterization. Synthetic routes to metal thiolates involve reaction of a thiolate salt with a metal halide, displacement of HNR_2 (commonly R = $SiMe_3$) from a metal amide using a thiol, or the reaction of thiol and metal halide in the presence of a base, typically Et_3N. The limited reports on the synthesis of $Sb(SR)_3$ to date have generally used either the salt[39,40] or amine[41] elimination routes where aromatic thiols are concerned, and the reaction of $SbCl_3$ and thiol in the presence of ammonia for alkyl derivatives.[42] We have employed both variations in this study

$$SbCl_3 + 3NaSBu^t \xrightarrow[-3NaCl]{MeOH} Sb(SBu^t)_3 \quad (\mathbf{1}, 70\%)$$

$$SbCl_3 + HSCH_2CF_3 \xrightarrow[-NH_4Cl]{NH_3/toluene} Sb(SCH_2CF_3)_3 \quad (\mathbf{2}, 70\%)$$

$Sb(SBu^t)_3$ has been prepared previously by the above route[42] and from the elimination of Me_3SiF from a mixture of SbF_3 and Me_3SiSBu^t.[43] Compound **1** is a white solid, mp 150 °C,

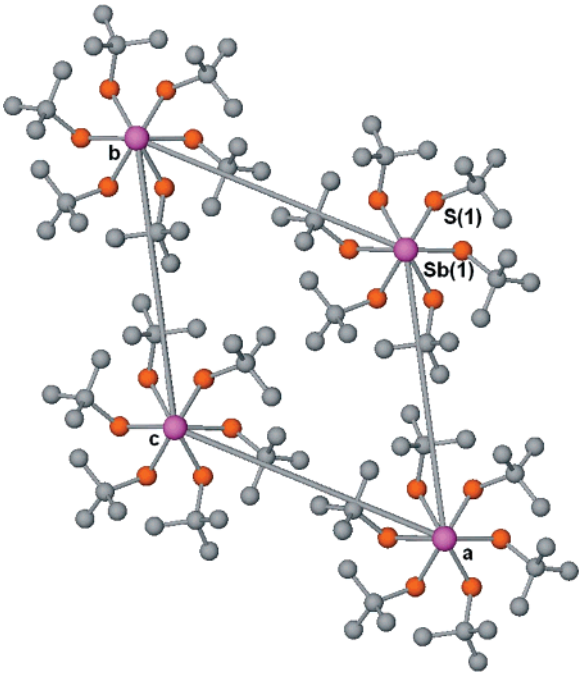

Figure 2. Unit cell of **1** viewed along *c*.

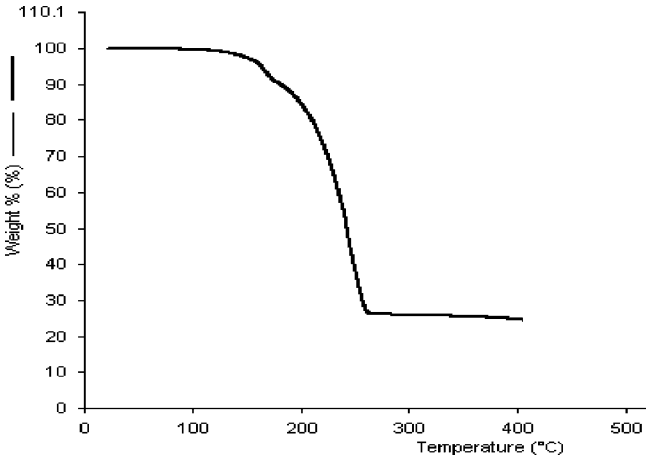

Figure 3. TGA of **1**.

whereas **2** is a clear oil; both have a pungent odor and are soluble in common organic solvents. **1** is air-stable, whereas **2** decomposed after a few days of exposure to air.

The structure of **1** is shown in Figure 1 and is the first structurally characterized antimony(III) alkylthiolate. The structure of $W(CO)_5[Sb(SBu^t)_3]$ has been reported[44] in which the thiolate acts as a 2e donor to tungsten, along with those of a small number of monomeric antimony arylthiolates $Sb(SAr)_3$ of varying degrees of steric crowding (Ar = Ph,[45] C_6H_4Me-4,[40] $C_6H_3Me_2$-3,5,[40] $C_6H_2Pr^i_3$-2,4,6[41]). **1** is pyramidal

(39) Block, E.; Oforiokai, G.; Kang, H. K.; Wu, J.; Zubieta, J. *Inorg. Chem.* **1991**, *30*, 4784.
(40) Clegg, W.; Elsegood, M. R. J.; Farrugia, L. J.; Lawlor, F. J.; Norman, N. C.; Scott, A. J. *J. Chem. Soc., Dalton Trans.* **1995**, 2129.
(41) Bochmann, M.; Song, X. J.; Hursthouse, M. B.; Karaulov, A. *J. Chem. Soc., Dalton Trans.* **1995**, 1649.
(42) Mehrotra, R. C.; Gupta, V. D.; Chatterjee, S. *Aust. J. Chem.* **1968**, *21*, 2929.
(43) Janzen, A. F.; Vaidya, O. C.; Willis, C. J. *J. Inorg. Nucl. Chem.* **1981**, *43*, 1469.
(44) Arif, A. M.; Chandler, D. J.; Jones, R. A. *J. Coord. Chem.* **1987**, *16*, 213.
(45) Peters, M.; Saak, W.; Pohl, S. *Z. Anorg. Allg. Chem.* **1996**, *622*, 2119.

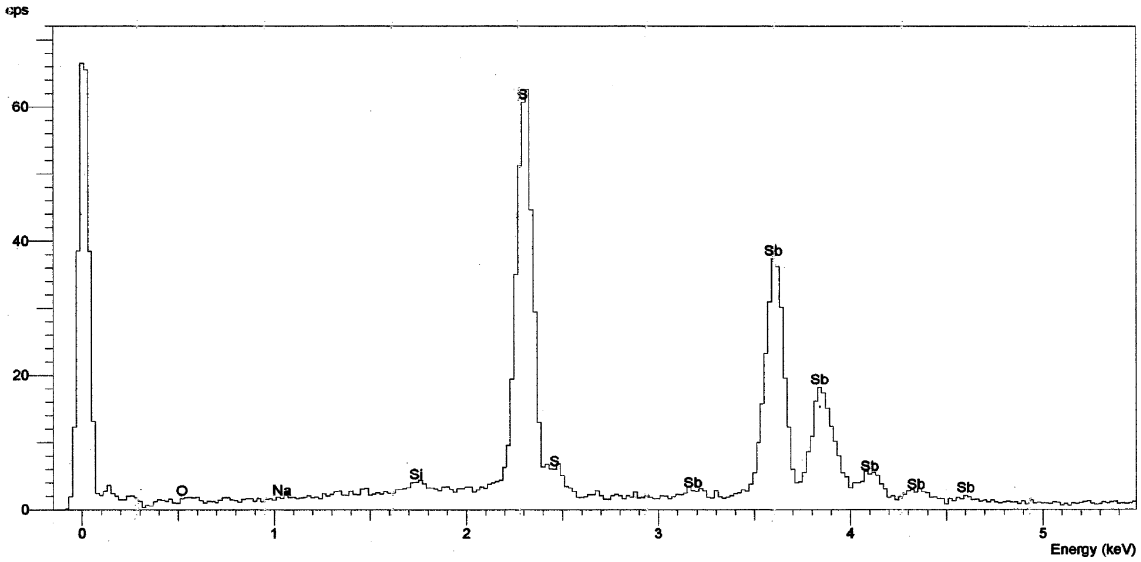

Figure 4. EDXS of the film deposited from precursor **1** on glass at 300 °C.

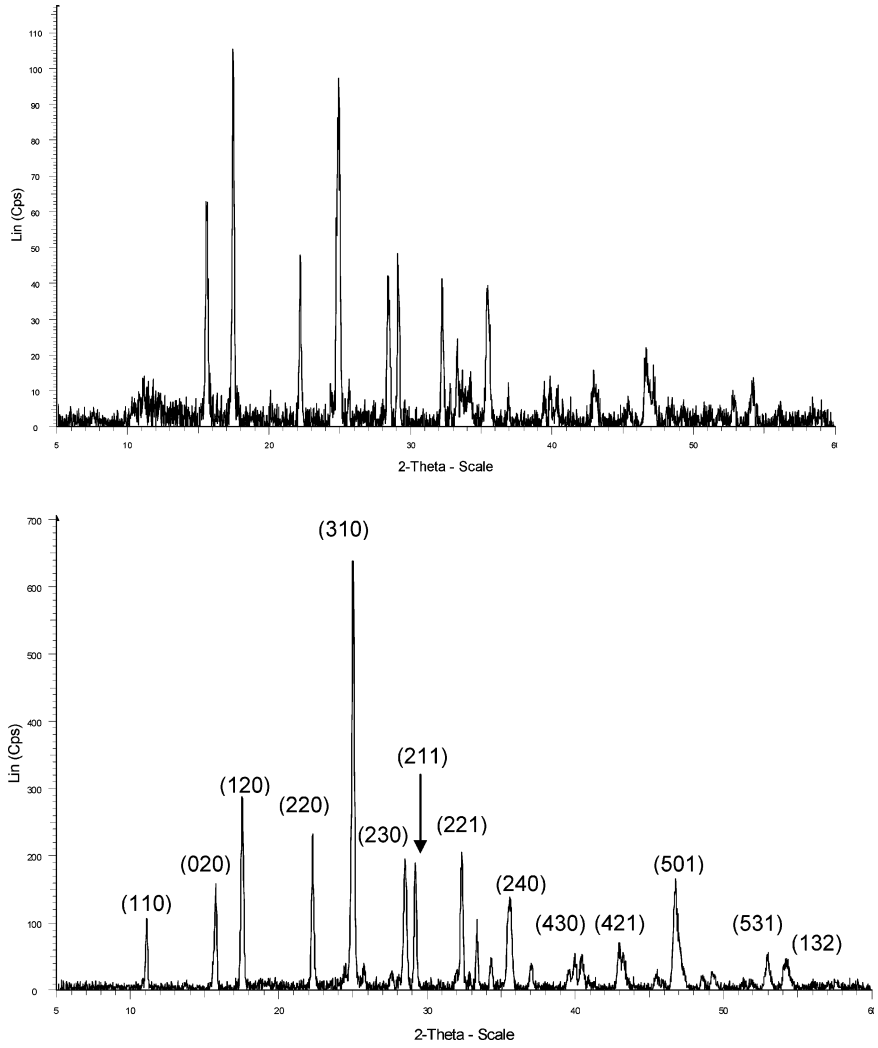

Figure 5. XRD patterns for the films deposited from **1** on (a) glass and (b) silicon at 300 °C. Indexing of the major lines is shown only for (a).

at the metal and is disordered (3:1) with respect to the "up" or "down" orientation of the pyramid; only the metrical data for the major component of the disorder are discussed. The molecule lies on a 3-fold axis so all Sb−S bonds are identical in length (2.4248(14) Å). The Sb−S bond is typical of other $Sb(SR)_3$ species, e.g., $Sb(SPh)_3$ 2.423(2) Å,[45] and is intermediate in comparison with the Sb−S bonds in $W(CO)_5$-$[Sb(SBu^t)_3]$, which incorporates one longer donor bond

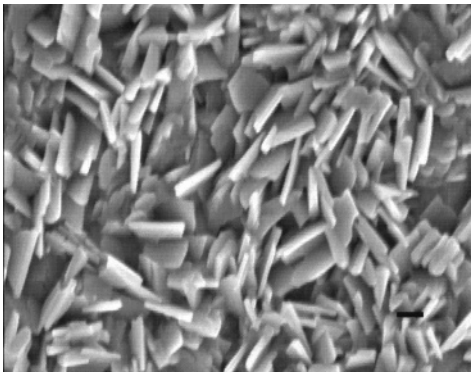

Figure 6. SEM of the film deposited from **1** on silicon; bar = 1 μm.

(2.492(1) Å) and two shorter terminal bonds (2.395(2) and 2.397(2) Å).[44] Symmetry also dictates that S−Sb−S angles in **1** are all identical (91.63(6)°), unlike the isoelectronic anions $[M(ER)_3]^-$ (M = Ge, Sn; E = S, Se), which show either narrow (86.7−92.8°) or wide (96.7−102.2°) E−M−E angles. Interestingly, however, the staggered nature of the t-butyl groups around the base of the S_3Sb pyramid (C−S−Sb−S torsion angles: 167.6, −100.7°) corresponds broadly to the conformation in $[M(ER)_3]^-$, which give rise to the narrow E−M−E angles. We have commented elsewhere of the interplay of conformation and bond angle, to which the interested reader is directed for a fuller discussion.[46] In the lattice, molecules of **1** form linear chains of antimony atoms with staggered SBu^t groups arranged in a propeller-like manner; the closest intermolecular S···Sb contacts are at the limit of the sum of the respective van der Waals radii (4.05 Å) (Figure 2).

Chemical Vapor Deposition Studies. Compounds **1** and **2** have been evaluated as precursors for the deposition of Sb_2S_3 films by LPCVD using a custom built hot-walled CVD reactor. TGA of **1** (Figure 3) shows a shoulder at ca. 150 °C, corresponding to the onset of sublimation. The total residual mass (ca. 25%) is lower than that for Sb_2S_3

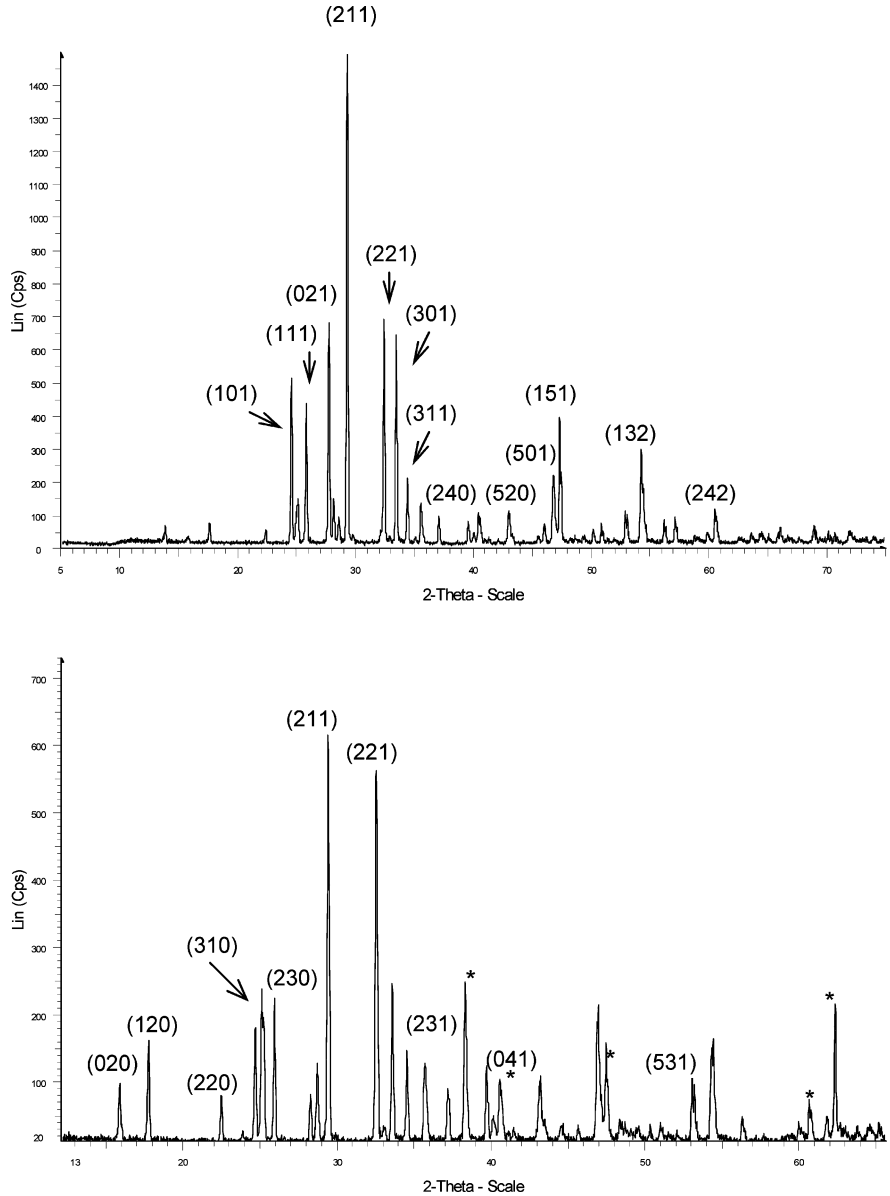

Figure 7. XRD patterns for the films deposited from **2** on (a) glass and (b) silicon at 450 °C. Indexing of the major lines is shown for (a), whereas for (b), the selective indexing identifies both the major lines and differences to the XRD of (a); reflections marked * in (b) are due to antimony metal (rhombohedral modification, PDF 05-0562) and can be indexed (from low 2θ upward) as (111), (104), (015), (116), and (107).

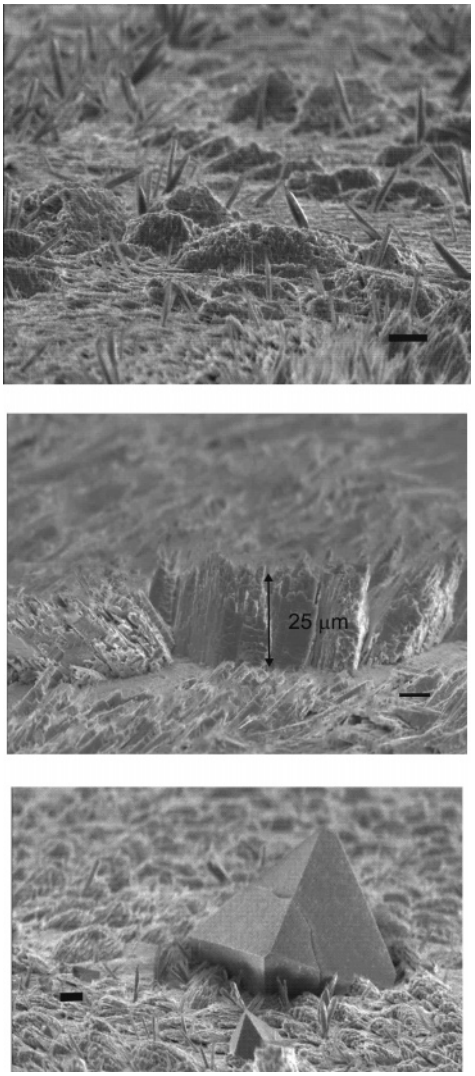

Figure 8. SEM of the film deposited from **2** on glass at 450 °C: (a) general view, (b) 73° tilt showing the approximate thickness of the island growths, and (c) isolated appearance of prismatic crystals of antimony metal (bar = 10 μm throughout).

(theoretical: 43.6%), again reflecting the volatility of Sb(SBu^t)$_3$ and mass loss due to sublimation. LPCVD studies were consequently carried out, setting the precursor temperature in the range 100−150 °C (between the start of sublimation and the onset of decomposition) and the substrate temperature from 300 °C, where the precursor has completely decomposed; details are given in Table 2. A marginally higher decomposition temperature was required for the fluorinated precursor (**2**), though in both cases, decomposition was incomplete and small amounts of precursor crystallized near the cool exhaust of the vacuum chamber.

Films derived from both precursors showed essentially identical EDXS spectra (Figure 4), showing the presence of antimony and sulfur. Only minor peaks due to the underlying substrate (Si, Na, O) were visible and peaks due to fluorine from **2** were absent; carbon contamination also seems to be negligible. Quantitative EDXS reveals a composition Sb:S

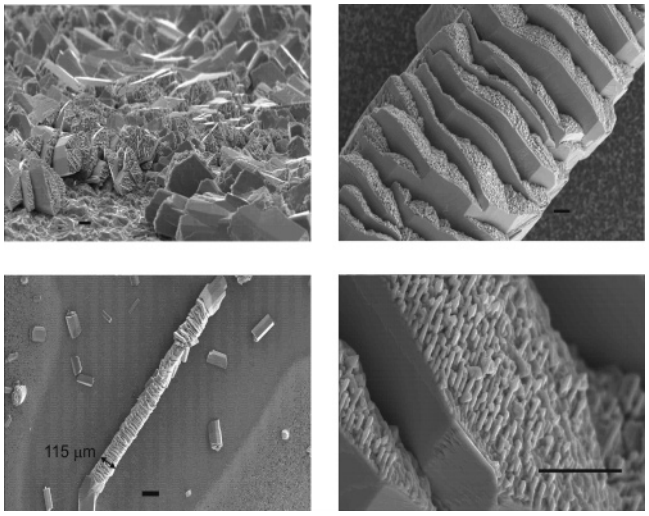

Figure 9. SEM of the film deposited from **2** on silicon at 450 °C: (a) general view showing the thin underlayer similar to that in Figure 8a and an overalyer of rodlike blocks (bar = 20 μm), (b) the rods as an assembly of plates (bar = 100 μm), magnification of the plates showing (c) their non-uniform cross-section and (d) their assembly from oriented wires (bar = 10 μm).

1.39 (i.e.$Sb_2S_{2.78}$), regardless of the substrate for **1**; for the films deposited from **2**, on glass, the Sb:S is 1:1.48, i.e., almost perfectly stoichiometric Sb_2S_3, whereas for those deposited from **2** on silicon, it is slightly sulfur-rich (1.55; $Sb_2S_{3.1}$).

Both films deposited from **1** were crystalline and could be indexed to the standard for stibnite Sb_2S_3 (orthorhombic, PDF 06−0474). Typical XRD patterns are shown in Figure 5, which highlight the difference influences of the underlying substrate. In neither case is there any significant preferential orientation of the crystallites, but both differ with respect to each other and the random stibnite sample, which has the most intense reflection as (221). SEMs for the two films are, however, essentially the same in appearance, thus only that for the film on a silicon substrate is presented (Figure 6). In both cases, platelets of ca. 2−3 μm in length of random orientation are seen.

Glancing angle XRD patterns for the films derived from **2** on both glass (Figure 7a) and silicon (Figure 7b) are similar, both to each other and the diffraction patterns of the corresponding films generated from precursor **1**. Both patterns can be indexed to stibnite (Sb_2S_3), though again there are differences in peak intensities. Somewhat surprisingly, whereas the major (221) reflection of the random sample is, along with (211), the dominant feature of the film on ordered silicon, the (211) reflection dominates on glass. Additionally, a small number of reflections not attributable to stibnite can be seen in Figure 7b, which are discussed later.

Although the XRD patterns for the two films derived from $Sb(SCH_2SF_3)_3$ show only minor influence from the underlying substrate, the SEM pictures of the two films reveal major differences in particle morphology. The film grown on glass shows relatively even coverage, with isolated islands of enhanced growth (Figure 8a). These islands show some vertical alignment, possibly the origin of the slight orientation preference seen in the XRD pattern (Figure 7a), with a thickness of ca. 25 μm (Figure 8b). In addition, a small

(46) Barone, G.; Hibbert, T.; Mahon, M. F.; Molloy, K. C.; Parkin, I. P.; Price, L. S.; Silaghi-Dumitrescu, I. *J. Chem. Soc., Dalton Trans.* **2001**, 3435.

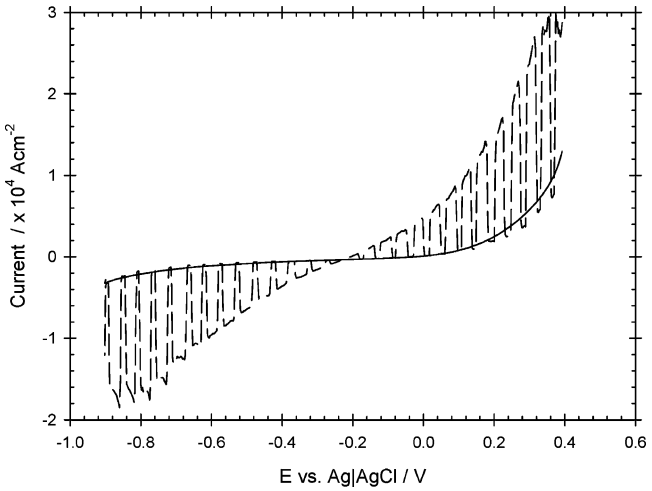

Figure 10. Cyclic voltammogram of Sb_2S_3 film deposited on fluorine-doped tin oxide (FTO) in 0.1 M Na_2SO_3(aq). The full line indicates dark current, and dashed line is the current response to chopped white light.

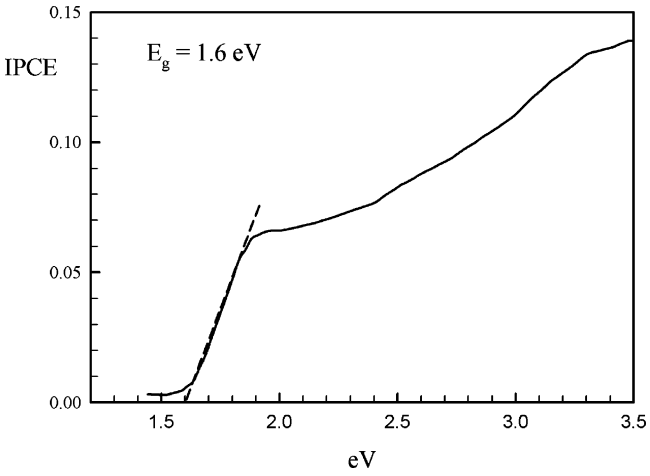

Figure 11. Photocurrent spectra of Sb_2S_3 film deposited on fluorine-doped tin oxide (FTO) in 0.1 M Na_2SO_3(aq), measured at +0.2 vs Ag|AgCl/V. Dashed line indicates extrapolation of band edge.

number of large isolated octahedral particles could be seen embedded into the surface of the film (Figure 8c), which EDXS indicate are antimony metal with some associated oxygen, presumably on the surface. These particles are as large as 70 μm × 70 μm around the base. Although the amount of this secondary material appears too small to impact the XRD pattern, peaks due to elemental antimony are seen in the XRD pattern of the film deposited on silicon (Figure 7b), discussed below. The formation of antimony particles has been reported previously when high temperatures (>500 °C) were used in the deposition of antimony oxide from antimony alkoxide $Sb(OR)_3$ precursors.[47]

A completely different morphology is observed when films are grown from precursor **2** on silicon wafers as the substrate. The overall composition of the film can be described as comprising two layers. The thin underlying layer presents a uniform coverage (Figure 9a) with a morphology very similar to the one seen in the films grown on a glass substrate from the same precursor (Figure 8a). Dominating this underlayer, however, is a second layer of rodlike blocks that are not seen when the films are grown on glass, giving an approximate thickness of 100 μm to the film. At higher magnification, these rodlike particles can be seen to be formed from an aggregation of plates (images b and c of Figure 9) with approximate dimensions 115 μm × 10 μm, although the thickness of the plates is by no means uniform (Figure 9c). These plates are themselves the result of a collection of microwires (Figure 9d) that can be seen protruding from the surface of the plates by ca. 1−2 μm. Surprisingly, although antimony metal is also present in this film by XRD (Figure 7b), the large octahedral particles evident in the films on glass (Figure 8c) were not seen. This could be an artifact of the area of the film studied by SEM or it could mean that the particles are of significantly smaller size and less evident in the presence of the large rod-shaped growths.

(47) Myers, C. P.; Haycock, P. W.; Pichot, M.; Horley, G. A.; Molloy, K. C.; Rushworth, S. A.; Smith, L. M. *Chem. Vapor Deposition* **2004**, *10*, 35.

Opto-electronic Characterization. The photovoltammetric response of the Sb_2S_3 film deposited on conducting glass is illustrated in Figure 10. It can be seen that, depending on the applied potential, both positive and negative photocurrents appear in response to the pulsed illumination. For doped semiconductors, photocurrents of only one sign are normally expected, corresponding to reaction of the photogenerated minority carriers at the interface. If the sample is *n*-type, the minority carriers are holes and the photocurrent is positive. Conversely, for *p*-type semiconductors, the minority carriers are electrons and the photocurrents are negative. The occurrence of photocurrents that change sign with applied bias indicates that the material is either intrinsic or, as is more likely in the present case, compensated. This means that the density of photogenerated electrons and holes exceeds the thermal density, and either carrier can be driven to the surface depending on the direction of the applied electric field.

The photon energy dependence of the photocurrent response of the film is shown in Figure 11. The external quantum efficiency or IPCE (incident photon conversion efficiency) is defined as the ratio of the photon flux onto the film to electron flux in the measured external circuit. No corrections were made for reflection losses. The response shows a clear onset at 1.6 eV, corresponding to the band gap of the Sb_2S_3 film. This value for the band gap agrees reasonably well with published values for the optical band gap of 1.78 eV for annealed Sb_2S_3 thin films.[20] Generally, photocurrent spectroscopy is a more reliable method than absorption spectroscopy for determining bandgaps, because it is less susceptible to errors arising from light scattering. The higher bandgaps that have been reported[30] for some films may be a consequence of quantization effects associated with small crystallite size.

4. Conclusions

Antimony thiolates $Sb(SR)_3$ (R = Bu^t (**1**), CH_2CF_3 (**2**)) can act as single-source precursors for the deposition of orthorhombic stibnite (Sb_2S_3) thin films at temperatures of 300 and 450 °C, respectively. The films are phase-pure, with a

stoichiometry of $Sb_2S_{2.78-3.10}$ by EDXS, though films derived from **2** show evidence of trace amounts of antimony metal. The morphologies of the deposited films show a strong dependence on both precursor and substrate, with the films deposited on Si from **2** showing a particularly striking rodlike growth from stacked platelets. The film deposited from **1** on conducting glass has a measured band gap of 1.6 eV (literature values ca. 1.78 eV) and is photoactive.

Acknowledgment. K.C.M and J.R.-C. thank the EPSRC and QinetiQ for grant GR/R95647/01. Mr H. R. Perrot (University of Bath) is also thanked for help with the SEM and EDXS analyses.

Supporting Information Available: X-ray crystallographic files, in CIF format, for compound **1**. This material is available free of charge via the Internet at http://pubs.acs.org.

CM070405J